INTERACTION OF A HOT JET WITH TWO COLD SIDE JETS

by

Nassira NOUALI and Amina MATAOUI *

Theoretical and Applied Laboratory of Fluid Mechanics, Faculty of Physics,
University of Science and Technology Houari Boumedienne, Algiers, Algeria

Original scientific paper
DOI: 10.2298/TSCI140310113N

Spreading of the multijet in terms of both the velocity and temperature field depends strongly on the flow type related to the velocity and temperature ratios between the cold side jets to the hot central one. This is the reason why the present work focuses on numerical investigation of non-isothermal three parallel non-ventilated turbulent plane jets. As well, it seems natural to pick as reference the available experimental data. The numerical predictions confirm the three types (A, B, C) of flow patterns given by the available flow visualization and reveal a fourth that will be called type D. The purpose of the present study is to explore the effect of the velocity ratio on the decay rates of the velocity and temperature in the fully developed region. It is found that the addition of side jets increase the rate of decrease of the centerline velocity for the flow of type A and decreases in the other cases. The effect of various types of flow on the rate of decrease of the velocity and the temperature in the fully developed flow region are investigated in details. This led to establish several correlations of the rate of decrease that play an important role in the diffusion of momentum and temperature.

Key words: *triple jets, turbulence, stagnation point, heat transfer, similarity*

Introduction

Parallel turbulent multijets are investigated experimentally and numerically by many researchers [1-12]. Turbulent rectangular jets are found in many engineering applications such as the propulsions of aircrafts, the dispersion of pollutants and the cooling of electronic packages. In multijet studies, the mutual influence of the adjacent jets on each other requires clear understanding and hence the three jets interaction studies becomes interesting. Such interaction is quite complex because each jet is subjected to a compression or an expansion of its shear layer. In view of these complexities, it is recommended to control the mixing between the jets and the entrainment of their surrounding flow. The aligned jets are also studied by other authors. The works of Salentey [13] and Lesieur [14] examined the configuration of three aligned injectors: a central jet of natural gas and two lateral jets of pure oxygen. These works investigated the dynamic and scalar fields as well as the behavior of oxy-flame depending on the dynamical and geometrical parameters of the burner study. The measurements made, for several velocities and different distances between the jets, allowed to point out the influence of these parameters on the stabilization of oxy-flame as well as modifying the topology and the characteristics of flows. In

* Corresponding author; e-mail: mataoui_amina@yahoo.fr

the case of flow resulting from jets and whatever the geometry of the injectors, it is possible to describe the overall flow through the three regions found previously in [1, 15, 16]:

– the combining zone is the region of the flow where the jets are not yet in complete interaction. The configuration of non-ventilated jets (where the space between the nozzles is confined by a wall) generates some vortices. This zone extends until the mixing point where the jets merge completely,
– the second zone is the merging region in which the jets are mixed and interact strongly. This area is quickly reached in the case of non-ventilated jets, [17]. The velocity and temperature profiles are characterized by several maxima and minima. This zone end is attained when the maximum value of the velocity is located on the central jet axis, and
– the third zone, called developed region, is located downstream of the combining point from which the combined jets recovers the single free jet behavior.

For the case of ventilated jets, there is another flow which penetrates at weak velocity between the neighboring jets breaking the vortices observed in the case of non-ventilated jets, [6]. Murai *et al*. [18] and Lin and Sheu [16] have compared these two types of flow configuration. In the vicinity of the nozzle, the authors noted that the decrease of the velocity and the spreading for the non-ventilated jets are attained before than that of the ventilated case. In the far field of the flow, they note that there is a little difference between the two cases. The second parameter to be defined before the design of the experimental set-up is the number of jets and their arrangement in space. In the case of slot jets, [15] showed that the rate of decrease of the average velocity along the central jet axis decreases when the number of jets augments. However, this fact becomes negligible for a greater number (more than 7) of jets. Raghunathan and Reid [5] reported that the increase of jets number induces noise reduction but has a minor effect on the momentum of the jet. The shape of the nozzle plays also a great role in the spreading of multijets. Indeed the use of plane jets (also called slot jets) is quite common in studies of multiple jets. The use of non-ventilated plane jets will lead to the development of re-circulation zones which are reduced in the case of round jets. Another major difference is due to the effect of nozzle's shape on the velocity and concentration distributions. Indeed, in the case of an axisymmetric jet, the decrease of the velocity depends on the dimensionless streamwise abscissa axis (x/a) but in the case of the slot jets, this decrease follows a law depending on the shape of the nozzle [19]. Some authors use triangular nozzles, [20] or even elliptical, [21] in order to improve the mixing of the jet with the surrounding flow. Krothapalli *et al.* [4] measured the mean velocity and Reynolds stresses for the configuration of the parallel rectangular jets. Laurence [22] studied the noise in a rectangular configuration of four jets. For a given spacing between the jets, it is still possible to modify the behavior of the jets mixing by inclining the nozzles. Becker and Booth [23] studied the effect of the inclination of two round jets. They confirm that, in the first region of the flow for the inclination between 15° and 45°, the jets will combine toward each other. After the merging point, they noted faster merging jets for large angles and in the far field they have found the values expected in the case of the single jet. Others applications of multijets interaction in engineering are discussed by Cao *et al.* [24], Tenchine *et al.* [25], and Svensson *et al.* [26]. The configuration chosen in present paper is an array of three parallel identical slot jets. This particular pattern is chosen, because it allows the deflection of the axis of each jet toward each other, generating a better mixing. Turbulent incompressible three jets flows are studied by Sforza *et al.* [27], Tanaka and Nakata [1], Krothapalli *et al.* [4], and Quinn [28]. These studies give much information for this type of flow interaction. The problem of interaction of hot and cold jets has many important applications such as the extinction of oil well fires. Sabbagh and Aly [29] show, experimentally, that the increase in flow velocities of the cold jet increases the cooling of the hot

jet and the spread of the temperature profile of the combined jet. Tanaka and Nakata [1] found three flow regimes (A, B, and C), depending on the ratio of side jet to central jet velocities. The dynamical and geometrical parameters are selected according to available data in [1] for the comparisons. The present study complements the work in [1] by considering several velocity ratios λ. This parameter is chosen to allow a comparative study of the decay rates of velocity and temperature. A similar study was carried out by Stanley *et al.* [30] for the case of a heated plane jet.

Methodology

Motion equations

The state of the flow is assumed steady in average and fully turbulent. The fluid (air) is incompressible with constant thermo-physical properties. The time-averaged equations, which define this flow, translate from the principles of conservation of the mass (eq. 1), momentum (eq. 2), and energy (eq. 3), coupled with the equations of the turbulence model:

$$\frac{\partial U_j}{\partial x_j} = 0 \tag{1}$$

$$\rho U_j \frac{\partial U_j}{\partial x_j} = -\frac{\partial P}{\partial x_i} + \frac{\partial}{\partial x_j}\left[\mu \frac{\partial U_i}{\partial x_j} - \rho \overline{u_i u_j}\right] \tag{2}$$

$$\rho U_i \frac{\partial T}{\partial x_i} = \frac{\partial}{\partial x_i}\left(\frac{\mu}{\mathrm{Pr}} \frac{\partial T}{\partial x_i} - \rho \overline{u_i \theta}\right) \tag{3}$$

where Pr = 0.71.

Four one-point closure models are checked in this study: the standard k-ε model, the RNG k-ε model, the SST k-ω model, and the RSM model. Svensson *et al*. [26] shows that this commonly used RANS turbulence models are able to predict accurately the mean velocity and the turbulence properties for multijets interaction. The standard k-ε model of Jones and Launder [31] based on the concept of Prandtl-Kolmogorov's turbulent viscosity is utilized in its high Reynolds number version. After that, Yakhot and Orszag [32] derived from the standard k-ε model, the RNG k-ε model by using the renormalisation group (RNG) methods. Menter [33] developed a turbulence model based on two-equation eddy-viscosity model: the shear stress transport k-ω model (SST k-ω model). The technique of the SST model is to use a k-ω formulation in the inner parts of the boundary layer and the k-ε model in the outer part of the boundary layer. To combine these two models together, the standard k-ε model has been transformed into equations based on k and ω, which leads to the introduction of a cross-diffusion term in the dissipation rate equation [34, 35]. Reynolds stress turbulence second moment closure (LRR-IP version) is based on transport equations for all components of the Reynolds stress tensor and the dissipation rate. It does not require the eddy viscosity hypothesis [36]. A preliminary study shows that both SST k-ω model and RSM model achieve the best predictions than the others models for the present configuration.

Numerical procedure

This study is performed by ANSY 14.0 Fluent CFD code, using the finite volume method. This numerical method requires a transformation of all equations in conservative form [37]), to convection, diffusion, and source terms. The boundary conditions are sketched in fig. 1.

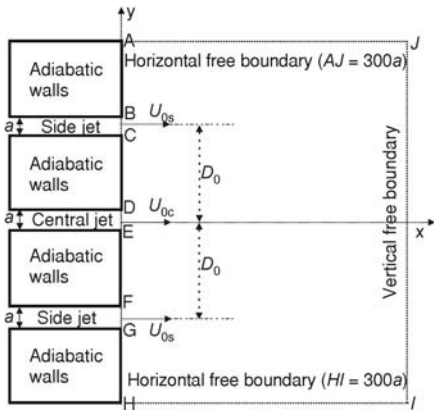

Figure 1. Geometry and boundary conditions

The ratio of the side jet to the central jet velocities is defined by $\lambda(\lambda = U_{0S}/U_{0C})$. The maximum Reynolds number of the side or the central one, $\mathrm{Re} = U_{0a}/\nu$, is set to 18800. At each jet exit (FG, ED, and CB) all variables are assumed constant.

– At the walls (HG, FE, DC, and BA) the mean velocity components (U, V), kinetic energy (k), dissipation (ε), and Reynolds stresses ($\overline{u_i u_j}$) are set to zero. The specific dissipation rate ω is kept to the asymptotic value proposed by Wilcox [31]. For the temperature, the walls are adiabatic.
– At the free boundaries (IJ, HI, and AJ), the static pressure and temperature are kept, respectively, at atmospheric pressure and ambient temperature. The free boundaries are far from the flow interaction in order to avoid their influences.
– The convection and diffusion terms are interpolated using the QUIK scheme for each variable ($\Phi = V, k, T, \overline{u_i u_j}, \varepsilon$ or ω) and the second order scheme is applied for pressure.

The pressure velocity coupling is achieved by the SIMPLE algorithm. The solution is supposed converged when the normalized residues of each variable are less than 10^{-7}. The source terms are linearized to ensure the stability of the solution.

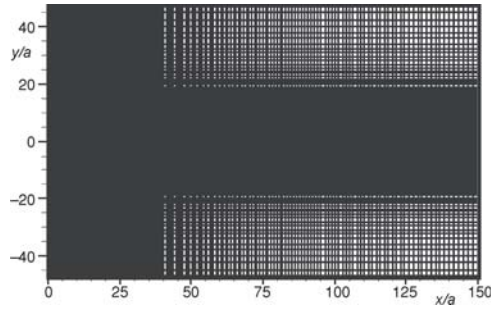

Figure 2. Typical grid (*N*x = 280 X, Ny = 150)

A 2-D structural non-uniform grids are generated. The meshes are refined near the wall where high gradients prevail. The influence of the grid distribution evidenced by the neighbouring region of the jets is deepened. Several meshes are tested, the choice fell on the mesh (fig. 2) which shows the same results as the finest one in order to economise computational time. This grid distribution is used in all following calculations based on the SST k-ω model, because the geometrical parameters of this study are not modified in this work. For the other turbulence models, others grids test are investigated.

Results and discussion

This work describes the behaviour of the interaction of three parallel jets. Both velocity and temperature fields are investigated. The reference [1] examine a large range of velocity ratio. As well, it seems natural to pick as reference this experimental work for the validation. The width of the nozzle of each jet is of 7 mm (a = 7 mm) and the distance between two neighbouring jets axis is D_0 ($D_0 = 11a$). For the thermal study, the heated central jet is set at TH and the cold side jets are kept at ambient temperature ($T_c = T_a$ =300 K).

The model validation

As mentioned above, the numerical predictions are compared with experimental available data, for several velocity ratios. Figure 3 illustrates the comparison of several RANS mod-

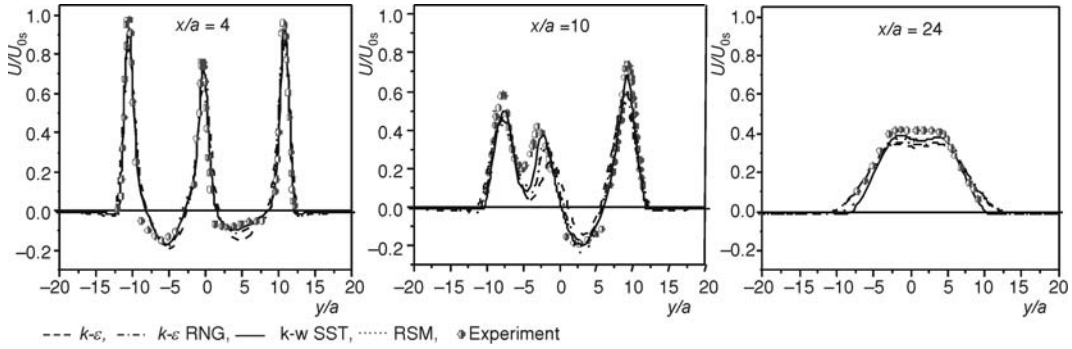

Figure 3. Turbulence model validation: normalised mean velocity (λ = 1.28)

els in the case of λ = 1.28. Eight cross-sections are selected.The results obtained by both RSM model and SST k-ω model are close to the experiments data of Tanaka and Nakata [1], while the k-ε model and the RNG k-ε model underestimate slightly the experimental data. The computations using the SST k-ω model predict the mean velocity with the best accuracy. These discrepancies are slightly more noticeable in the areas of reverse flow, which may be explained by hot-wire technique that is not suitable for recirculating flow. Unlike the flow of type A, the flows of type B and C (λ increases) will delay the merger jets, reduce the velocity of the central jet and increases those of the sides jets. As we noted above, in what follows, the one point closure SST k-ω model is used to save computational time, since it gives almost the same results as the RSM model for the mean velocity and the mean temperature.

Mean flow structure

Tanaka and Nakata [1] studied only the effect of the velocity ratio λ on the interference region by the detailed measures of the flow field variables. They observed three regimes of flow depending on the velocity ratio λ. Each flow pattern type are evidenced by visualisation picture achieved by the oil film method. A good agreement is obtained with the streamlines contours (fig. 4) and the location of stagnation points (tab. 1) computed on the basis of the k-ω SST model. Furthermore, a fourth type of flow pattern is highlighted in this study.

Table 1. Stagnation points (λ = 1.28)

	Stagnation points	x_s/a upper	x_s/a lower
Present study	k-ω SST	16.75	9.90
	RSM	15.17	8.94
	k-ε RNG	14.49	9.70
	k-ε	13.34	9.66
Experiment	Tanaka *et al.* [1]	18.70	9.89

The type A ($\lambda < 0.707$)

The central jet is more dominant, thus the side jets are driven and absorbed toward the central jet edges. Two ranges of λ characterise this type of interaction:

– for $0.395 \le \lambda < 0.707$, two secondary eddies appear between the two main re-circulation zones. Two symmetrical stagnation points, on each side of the central jet axis, characterise this range of λ, and
– for $\lambda < 0.395$ no stagnation point is observed, the secondary vortices disappear, because the momentum of the central jet exceeds that of the side one, therefore it completely absorbs the side jets.

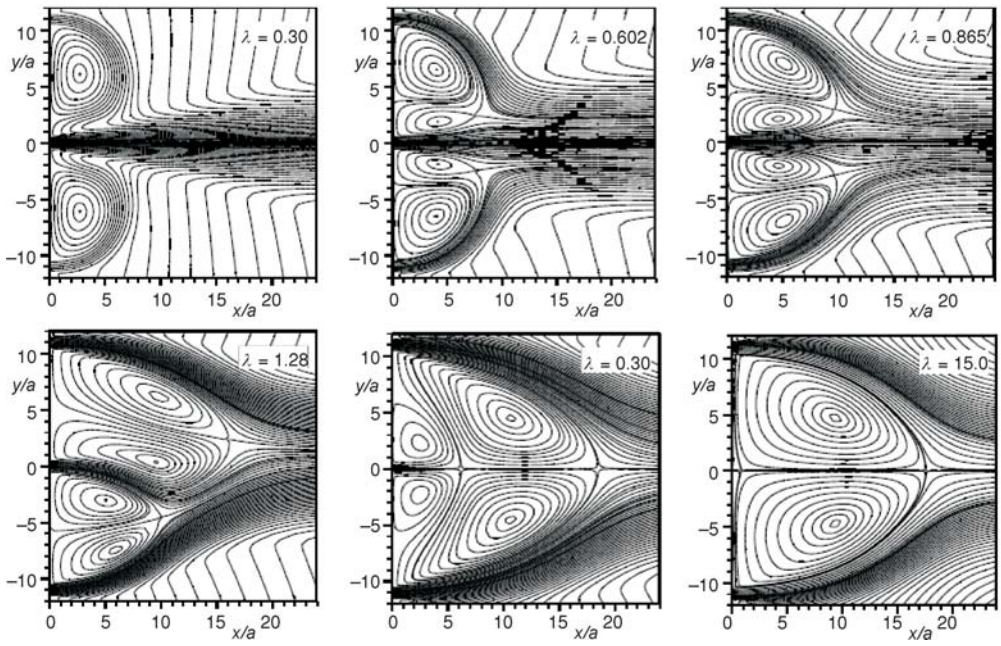

Figure 4. Computed streamlines contours (*k*-ω SST model)

The type B ($0.707 \leq \lambda < 1.11$)

The re-circulation zones are composed of two symmetrical counter-rotating vortices. The central jet is sucked out by the lateral jets. The maximum velocity is not located along the central axis. On each side of the central jet axis, two symmetrical stagnation points are observed.

The type C ($1.2 < \lambda < 2$)

With increasing the velocity of the side jets, the re-circulation zones composition become difficult to define. The central jet is rapidly deviated to one side of one lateral jet, where the first stagnation point occurs downstream. This combined flow joined the second lateral jet at the second stagnation point. The flow is asymmetric and merging jets is slower as in the preceding case. It also should be noted that at the transition between this case and the previous one, the central jet oscillates between the two side jets which generates some very noisy configurations and unsteady behavior [1, 13].

Type D ($2 < \lambda < 20$)

For $\lambda = 15$, a reversed flow occurs in the central region of two outside jets before combining and completely overcomes the central jet and the first stagnation point is pushed back upstream. Unlike the previous case, it should be pointed that the structure of the flow becomes symmetric and the two stagnation points are located on the central jet axis ($\lambda = 3$). The structure of the plane parallel dual jet flow (fig. 4) is obtained progressively with the increase of λ: this is a phase of slow transition to the two jets flow, diminishing the influence of the central jet.

The analysis of streamlines allows to propose a new classification which is shown schematically in fig. 5. The type A is characterized by no stagnation point ($\lambda < 0.395$). The schematic representation of this type of interaction is more detailed than that of Tanaka and Nakata [1]. The

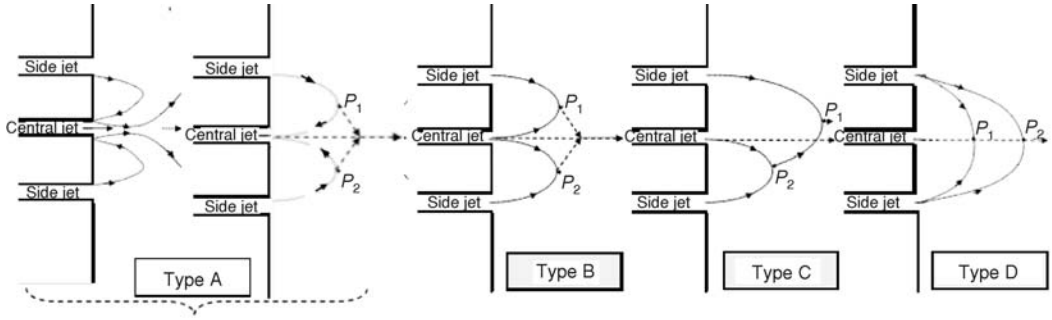

Figure 5. New flow patterns classification

type B are characterized by two stagnation points (P1, P2) located symmetrically to the axis of the central jet. The type C is characterized by two stagnation points (P1, P2) located asymmetrically to the central jet axis. The type D is characterized by two stagnation points (P1, P2) located on the central jet axis. For the validation, a test case of $\lambda = 1.28$ is presented in tab. 1. It is found that the best results are those of the *k-ω* SST model. The study of Tanaka and Nakata [1] is conducted using both hot wire and Pitot tube which are subject to serious errors [8].

Developed region

In the fully developed flow region, after the merging point, the structure of single jet flow is recovered, fig. 6(a). The crosswise distributions of streamwise velocity $U(y)$, at x/a = 128, has the same shape for each velocity ratio. For each case, the maximum velocity value U_m and the half width $y_{0.5}$ of the jet are used to plot dimensionless profile ($U/U_m = f(y/y_{0.5})$). The velocity distributions at $\lambda = 0.3$, 0.602 and 0.865 fall on one common curve with that of a single jet, fig. 6(a). The profiles show a symmetrical velocity with respect to the central jet axis. The highest velocity is situated on the central axis of the centre jet. The CFD results follow the Gaussian curve in that they match the Goertler [38] profile in the inner part of the flow and the Tollmien [39] curve in the outer part of the flow, up to a position around ±1.5 in the dimensionless abscissa axis, when the plots begin to separate. An important point to note is that all the CFD results lie between the two theoretical curves. At $\lambda = 1.28$, fig. 6(a) shows that the symmetrical pattern is broken for the jet and consequently the point of maximum velocity will deviate from the central jet axis. It is also found that the additional jets on each side of the central jet imply its

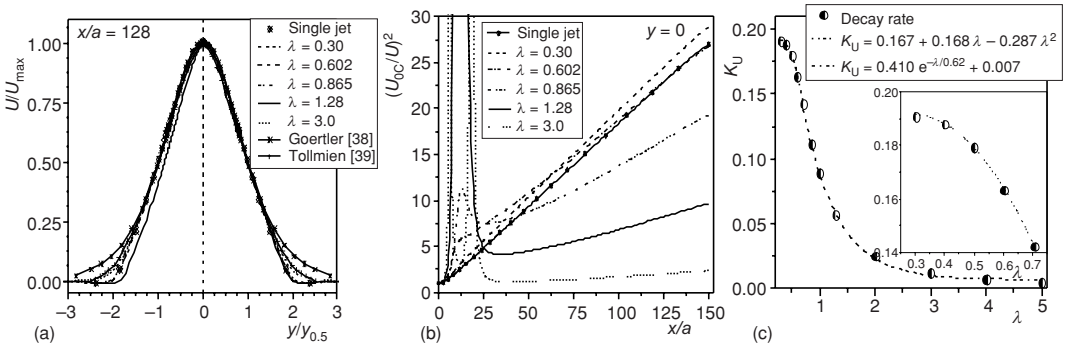

Figure 6. Effect of λ on the velocity profiles

compression transversely. Therefore, the spreading of the jet of types C is less than that of the single jet.

Centreline evolution

Pani and Dash [15] showed, in the case of slot jets, that the decay rate of the mean velocity along the central jet decreases when increasing the number of jets. Figure 6(b) shows, in comparison with the single jet, that the rate of decrease of the mean velocity along the central jet will increase as the flow is of type A and decreases in the case of type B, C, and D. The different values of the slope of decrease (K_U) are obtained by fitting the far-field data, using linear regression, to $(U_{0C}/U)^2 = K_U(x/a) + C_U$ and are plotted *vs*. λ fig. 6(c). The plotted curve is correlated with two distinct functions:

$$K_U = 0.167 + 0.168\,\lambda - 0.287\,\lambda^2 \qquad \text{for } \lambda \le 0.707 \tag{4}$$

$$K_U = 0.41\ e^{-\lambda/0.62} + 0.007 \qquad \text{for } \lambda \ge 0.707 \tag{5}$$

The first describing the evolution of K_U for a flow of type A and the second one for the other types of flow. This confirms the fact that the decay rate of the mean velocity also depends on the type of flow. When λ increases the decay rate (K_U) tends towards an asymptotic value corresponding to the case of dual jets.

Temperature field

The purpose of this paper is about the heat transfer process by jets. One considers a hot central jet between two cold side jets, for several velocity ratios . Some temperature differences between the hot jet and the cold jet (10 °C ≤ T ≤ 50 °C) are considered. The analysis of fig. 7 shows that the presence of the hot fluid from the central jet is highlight by the maxima of the iso-

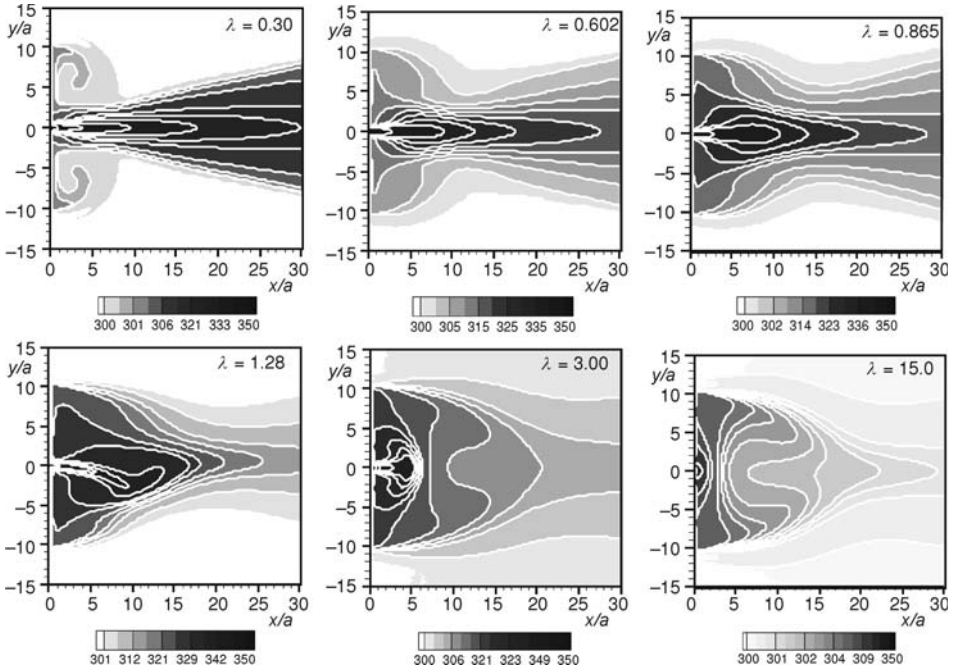

Figure 7. Mean temperature contours for different

therms in the vicinity of the nozzle. The dispersion of the temperature is controlled by the vortices. The isotherms follow the behaviour of the streamlines contours at the outlet and near the nozzles. The hot jet spreads between the two cold side jets except for the flow of type D where the hot jet is completely surrounded by the cold jets.

Temperature evolution in fully developed region

Figure 8(a) depicts the predicted temperature profiles in the self-similar zone as resulting from the several values of λ. These simulating curves match very closely the Ramaprian *et al.* [40] experimental data in the inner part of the flow; up to a position around ±1.5 in the dimensionless abscissa axis, the plots begin to separate. However, the temperature curve of the type D is superposed to the Ramaprian *et al.*[40] profile. For purposes of comparison, figs. 6(a) and 8 show that the calculated curves for the dimensionless velocity and dimensionless temperature at the same cross-section coincide. The normalized temperature profiles are similar for several T. Therefore, the temperature spreading of the jet of types (A, B, and C) is less than that of the single jet. Furthermore, that of the jet type C is the smallest one fig. 8(b). At λ = 1.28, fig. 8(a) and (b) show asymmetrical pattern for the jet and, consequently, the point of maximum temperature will deviate from the central jet axis. The plots match the dimensionless profiles and begin to separate up to position +1.5. This is due to gradient of temperature. This simulating curve matches very closely the Goertler shifted profile in the inner part of the flow, whereas in the outer part it shows a good fit to the Tollmien shifted profile.

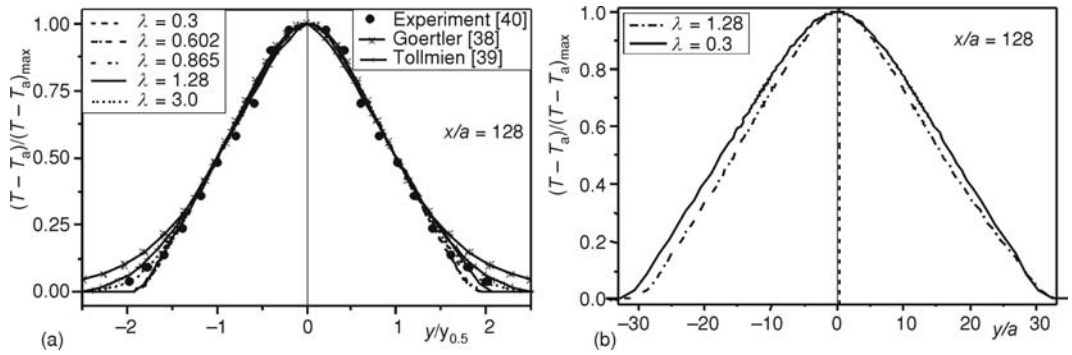

Figure 8. Self-similarity profiles for 10 °C ≤ ΔT ≤ 50 °C

Centerline temperature evolution

The dimensionless parameter $\Delta\Theta$($\Delta\Theta = (T - T_a)/(T_H - T_a)$) is the increment of temperature at the jet centerline due to the interaction of cold side jets with the central hot jet as compared to the ambient temperature. The influence of the velocity ratios is illustrated in fig. 9(a) which show $\Delta\Theta^{-2}$ at different stations x/a downstream of the central jet exit. Figure 9(a) shows that the rate of decrease of the mean temperature along the central jet increases when the velocity ratio λ increases.

The different values of the decay rate (K_T) are obtained by fitting the far-field data, using linear regression, to $[(T - T_a)/\Delta T]^{-2} = K_T(x/a) + C_T$ and are plotted *vs.* λ. The curve representing the decay rate *vs.* λ is correlated with a power function (eq. 6), see fig. 9(b).

$$K_T = 0.128 + 0.194\,\lambda^{2.198} \tag{6}$$

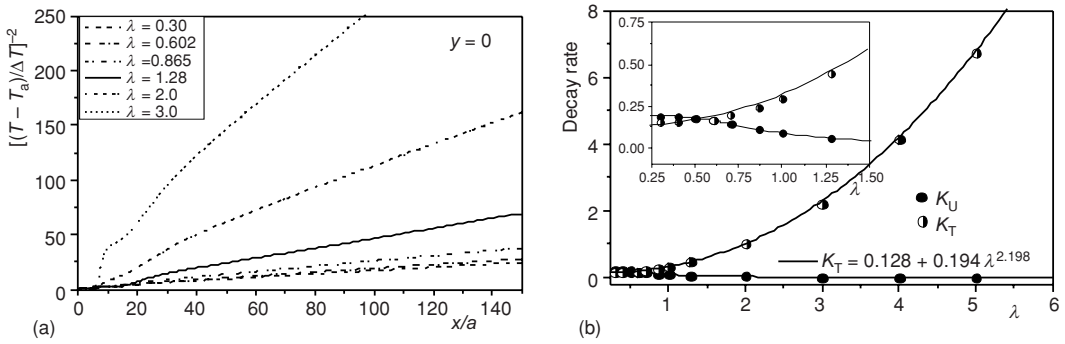

Figure 9. Effect of λ on the temperature decay rate

For the flow of type A ($\lambda < 0.71$), the decay rate (K_T) varies slightly, which means that the low velocities of the cold side jets have a minor effect on the temperature profiles in the combined region. For the other types of flow, the increase in the decay rate of temperature as a function of λ is large. Therefore, the flow of type D appears as the best alternative to cool the central hot jet in the combined region. This result is in agreement with that of [29].

For comparison, fig. 9(b) shows the decay rates of the velocity and temperature. It appears that the decay rates of temperature are larger than those for the velocity at each velocity ratio ($\lambda > 0.5$) for the flow of type A, B, C, and D, indicating that turbulent scalar transport occurs at a faster rate than turbulent momentum transport. For the flow of type A ($\lambda < 0.5$) the opposite phenomenon occurs indicating that the turbulent momentum diffuses a little more than the scalar field.

Conclusions

The flow patterns in the three parallel jets change with the variation of the nozzle velocity jet exit ratio ($\lambda = U_{0S}/U_{0C}$). Four RANS turbulence models are tested for several λ. In comparisons with the available experimental data, the SST k-ω model and RSM model results are better than those of the standard k-ε model and RNG k-ε model. A new classification of the flow pattern is highlighted. Four types of flow are identified instead of the three cited in the literature. In comparison with a single free plane jet, it is found that the addition of side jets increases the rate of decrease of the centerline velocity for the flow of type A and decreases in the other cases. The centerline profiles of the mean temperature are similar for several temperature gaps ΔT at each velocity and temperature ratio. For the type C, the symmetrical pattern is broken then both velocity and temperature maximum are shifted from the central jet axis in the developed region. Some correlations of the decay rate of both velocity and temperature along the central jet axis in the developed region are found in this paper. These correlations show that the types of flow play a major role on the momentum and temperature diffusion. The temperature correlation also confirms that the flow of type D appears as the best alternative to cool the hot central jet in the combined region. The turbulence characteristics of the multijet by the Reynolds stress models will be deepened in the future.

Nomenclature

a – slot nozzle width, [m]
D_o – distance between two nozzles, [m]
k – turbulent kinetic energy, [m^2s^{-2}]
P – mean pressure, [Pa]
Re – Reynolds number
T – mean temperature, [K]

U – mean velocity in the x-direction, [ms^{-1}]
U_i, U_j – velocities components, [ms^{-1}]
U_0 – jet exit mean velocity, [ms^{-1}]
U_{0C} – central jet exit velocity, [ms^{-1}]
U_{0S} – side jet exit velocity, [ms^{-1}]
$\overline{u_i u_j}$ – Reynolds stress component, [m^{2}s^{-2}]
V – mean velocity in the y-direction, [ms^{-1}]
x, y – streamwise and transverse co-ordinate, [m]
x_S – stagnation point, [m]
$y_{0.5}$ – half width of the jet, [m]

Greek symbols

ε – dissipation of turbulent energy, [m^{2}s^{-3}]
θ – temperature fluctuation, [K]
λ – nozzle discharge velocity ratio
μ – dynamic viscosity, [kgm^{-1}s^{-1}]
ρ – density of air, [Kgm^{-3}]
ω – specific dissipation rate, [s^{-1}]

Subscripts

C – cold temperature
H – hot temperature
t – turbulent
w – wall

References

[1] Tanaka, E., Nakata, S., The Interference of Two-Dimensional Parallel Jets (3rd report, The Region Near the Nozzles in Triple jets), *Bulletin of the JSME, 18* (1975), 124, pp. 1134-1141
[2] Loukarfi, L., *et al*., Improvement of Thermal Homogenization using Multiple Swirling Jets, *Termal Science, 16* (2012), 1, pp. 239-250
[3] Al Mubarak, A. A., *et al*., Heat Transfer in Channel with Inclined Target Surface Cooled by Single Array of Centered Impinging Jets, *Thermal Science, 17* (2013), 4, pp. 1195-1206
[4] Krothapalli, A., *et al*., On the Mixing of a Rectangular Jet, *Journal of Fluid Mechanics, 107* (1981), June, pp. 201-220
[5] Raghunathan, S., Reid, I. M., A Study of Multiple Jets, *AIAA Journal, 19* (1981), 1, pp. 124-127
[6] Elbanna, H., *et al*., Investigation of Two Plane Parallel Jets, *AIAA Journal, 21* (1982), 7, pp. 986-991
[7] Jung, J. H., Yoo, G. J., Analysis of Unsteady Turbulent Triple Jet Flow with Temperature Difference, *Journal of Nuclear Science and Technology, 41* (2004), 9, pp. 931-942
[8] Nasr, A., Lai, J. C. S., Comparison of Flow Characteristics in the Near Field of Two Parallel Plane Jets and an Offset Plane Jet, *Physics of Fluid, 9* (1977), 10, pp. 2919-2931
[9] Kimura, N., *et al*., Experimental Investigation on Transfer Characteristics of Temperature Fluctuation from Liquid Sodium to Wall in Parallel Triple-Jet, *International Journal of Head and Mass Transfer, 50* (2007), 9, pp. 2024-2036
[10] Tokuhiro, A., Kimura, N., An Experimental Investigation on Thermal Striping Mixing Phenomena of a Vertical Non-Buoyant Jet with Two Adjacent Buoyant Jets as Measured by Ultrasound Doppler Velocimetry, *Nuclear Engineering and Design, 188* (1999), 1, pp. 49-73
[11] Yamamoto, K., Hishida, K., Quantitative Visualisation of Turbulent Mixing in Parallel Triple Plane Jets, *Experimental Heat Transfer Fluid Mechanics and Thermodynamics* (2001), 2, pp. 1029-1034
[12] Buddhika, N. H., A Numerical Study of Heat Transfer Performance of Oscillatory Impinging Jets, *International Journal of Heat and Mass Transfer, 52* (2009), 1, pp. 396-406
[13] Salentey, L., Experimental Study of the Behavior of Burners with Separated Jets, Application for Combustion of Clean Natural Gas and Oxygen (in Franch), Ph. D. thesis, Faculty of Science and Technoloy, University of Rouen, France, 2002
[14] Lesieur, C., Moddeling of Turbulent Premixed Combustion in the Burner with Separated Jets Applied for Oxy-Flame Stabilisation (in French) Natinal Institute of Applied Scences, Rouen, France, 2003
[15] Pani, B. S., Dash, R. N., Three-Dimensional Single and Multiple Free Jets, *Journal of Hydraulic Engineering, ASCE, 109* (1983), 2, pp. 254-269
[16] Lin, Y. F., Sheu, M. J., Interaction of Parallel Jets, *AIAA Journal, 29* (1991), 9, pp. 1372-1373
[17] Marsters, G. F., Interaction of Two Plane Parallel Jets, *AIAA Journal, 15* (1977), 12, pp. 1756-1762
[18] Murai, K., *et al.*, An Experimental Study on Confluence of Two Dimensional Jets, *Bulletin JSME, 19* (1976), 134, pp. 956-964
[19] Grandmaison, E. W., Zettler, N. L., Turbulent Mixing in Coflowing Plane Jets, *The Canadian Journal of Chemical Engineering, 67* (1989), 6, pp. 889-897
[20] Koshigoe, S., *et al*., Initial Development of Non Circular Jets Leading to Axis Switching, *AIAA J, 27* (1989), 4, pp. 411-419

[21] Schadow, K. C., *et al.*, Combustion-Related Shear-Flow Dynamics in Elliptic Supersonic Jets, *AIAA Journal, 27* (1989), 10, pp. 1347-1353
[22] Laurence, J. C., Turbulence Studies of Rectangular Slotted Noise-Suppressor Nozzle, NASA Technical Note D-294, 1960
[23] Becker, H. A., Booth, B. D., Mixing in the Interaction Zone of Two Free Jets, *AIChE J., 21* (1975), 5, pp. 949-958.
[24] Cao, Q., *et al.*, Numerical Investigation on Temperature Fluctuation of the Parallel Triple-Jet, *Nuclear Engineering and Design, 249* (2012), Aug., pp. 82-89
[25] Tenchine, D., et al., Experimental and Numerical Studies on Mixing Jets for Sodium Cooled Fast Reactors, *Nuclear Engineering and Design, 263* (2013), pp. 263-272
[26] Svensson, K., *et al*., Numerical and Experimental Investigation of the Near Zone Flow Field in an Array of Confluent Round Jets, *International Journal of Heat and Fluid Flow, 46* (2014), Apr., pp. 127-146
[27] Sforza, P. M., *et al*., Studies on Three-Dimensional Viscous Jets, *AIAA Journal, 4* (1966), 5, pp. 800-806
[28] Quinn, W. R., Turbulent Free Jet Flows Issuing from Sharp-Edged Rectangular Slots: The Influence of Slot Aspect Ratio, *Experimental Thermal and Fluid Science, 5* (1992), pp. 203-215
[29] Sabbagh, J. A., Aly, M. S., Interaction of Two-Dimensional Hot Jet and Two-Dimensional Cold Jets, AIAA 93-3122, *Proceedings*, 24th Conference Fluid Dynamics, 1993, pp. 1-9
[30] Stanley, S. A., *et al*., A Study of the Flow Field Evolution and Mixing in a Planar Turbulent Jet Using Direct Numerical Simulation, *J. Fluid Mech, 450* (2002), Jan., pp. 377-407
[31] Jones, W. P., Launder, B. E., The Prediction of Laminarization with a Two-Equation Model of Turbulence, *International Journal of Heat Transfer, 15* (1972), 2, pp. 301-304
[32] Yakhot, V., Orszag, S. A., Renormalization Group Analysis of Turbulence. I. Basic Theory, *J. Sci. Comput, 1* (1986), 1, pp. 3-51
[33] Menter, F. R., Zonal Two Equation k-ω Turbulence Models for Aerodynamic Flows, 24th Fluid Dynamics Conference, AIAA, Orlando, Fla., USA, 1993
[34] Menter, F. R., Two-Equation Eddy-Viscosity Turbulence Models for Engineering Applications, *AIAA Journal, 32* (1994), 8, pp. 1598-1605
[35] Wilcox, D. C., Turbulence Modelling for CFD, DCW Industries Inc, La Canada, Cal., USA, 1993
[36] Launder, B. E., *et al*., Progress in the Developments of a Reynolds-Stress Turbulence Closure, *J. Fluid Mechanics, 68* (1975), 3, pp. 537-586
[37] Patankar, S. V., *Numerical Heat Transfer and Fluid Flow*, Series in Computational Methods in Mechanics and Thermal Sciences, Hemisphere Publishing Corp. & Mc Graw Hill, New York, USA,1980
[38] Goertler, H., Berechnung von Aufgaben der freien Turbulenz auf Grund eines neuen Naherungsansatzes, Z.A.M.M., 22 (1942), 5, pp. 244-254
[39] Tollmien, W., Berechnung turbulenter Ausbreitungsvorgange. Z.A.M.M., *6* (1926), 6, pp. 468-478. (English translation, N.A.C.A. TM, 1085, 1945)
[40] Ramaprian, B. R., Chandrasekhara, M. S., LDA Measurements in Plane Turbulent Jets, *Transactions of the ASME – Journal of Fluids Engineering, 107* (1985), 2, pp. 264-271

Paper submitted: March 10, 2014
Paper revised: September 9, 2014
Paper accepted: September 15, 2014